

Research Article

Electrocatalytic Performance of Pt–Ru–Co/MC Electrode for Methanol Oxidation in Non-membrane Power System

P. Ramar¹, M. Chitralkha^{2*}

¹Department of Chemistry, Government Arts College, Ariyalur-621 713. India.

²Department of Chemistry, D G Government Arts College, Mayiladuthurai-609001. India.

*Corresponding author's e-mail: chitralkhaprof@yahoo.com

Abstract

The present work represents the mesoporous carbon supported Pt₁₀₀, Pt₅₀Ru₅₀, Pt₅₀Co₅₀, Pt₆₀Ru₂₀Co₂₀, Pt₆₀Ru₁₀Co₃₀ and Pt₆₀Ru₃₀Co₁₀ catalysts with different mass ratios have been prepared by Pechini method. The crystallite size, lattice parameter, composition, and particle size of metals in the electrocatalysts were determined by XRD, EDX and TEM techniques, respectively. X-ray diffraction analysis showed that catalysts have a Pt face-centred cubic (fcc) structure with crystallite size of 3–4.5 nm. The EDX results of the binary Pt–Ru/MC and Pt–Co/MC and the ternary Pt–Ru–Co/MC catalysts were extremely close to the nominal values, indicating that the metals were loaded onto the mesoporous carbon support without any obvious loss. The size of catalyst nanoparticles was observed via TEM and showed an average diameter of 3.3 nm. The electrocatalytic activities of Pt₁₀₀/MC, Pt₅₀Ru₅₀/MC, Pt₅₀Co₅₀/MC, Pt₆₀Ru₂₀Co₂₀/MC, Pt₆₀Ru₁₀Co₃₀/MC and Pt₆₀Ru₃₀Co₁₀/MC catalysts were investigated in terms of CV and CA. The electrochemical results showed that the catalytic activity in 1.0 M MeOH + 0.5 M H₂SO₄ solution at 0.5 V vs. Ag/AgCl exhibits the following sequence: Pt₆₀Ru₃₀Co₁₀/MC > Pt₆₀Ru₂₀Co₂₀/MC > Pt₆₀Ru₁₀Co₃₀/MC > Pt₅₀Ru₅₀/MC > Pt₁₀₀/MC > Pt₅₀Co₅₀/MC. This clearly indicates that the performance of the ternary Pt₆₀Ru₃₀Co₁₀/MC electrocatalysts for methanol electro-oxidation is better than that of the binary Pt₅₀Ru₅₀/MC and Pt₅₀Co₅₀/MC electrocatalysts due to the promoting function of Co. In addition, its CO-tolerance is better than that of the Pt₅₀Ru₅₀/MC and Pt₅₀Co₅₀/MC catalysts. The high activity of Pt₆₀Ru₃₀Co₁₀/MC electrocatalyst was also observed on membraneless methanol fuel device, which was consistent with the half-device measurements.

Keywords: Methanol; Non-membrane power system; Platinum; Ruthenium; Cobalt; Electrocatalysts.

Introduction

Methanol is a mesoporous carbon-neutral, sustainable fuel that can be produced in great quantity through the fermentation of agricultural products or biomass. It also possess many unique properties including low toxicity and ease in handling and transportation compared to other power device. Methanol fuel will not change the natural balance of carbon dioxide into the atmosphere in contrast to the cost of fossil fuels. Methanol oxidation reaction provides many adsorbed intermediates, byproducts and the cleavage of C–C bond is difficult at low temperature, thus, extra difficult to illuminate accurately the mechanism of methanol electro-oxidation. It is very essential to develop new catalysts through towering catalytic activity for ethanol oxidation. Elevated activity and stability of Pt, particularly beneath acidic

nature, formulate it an appropriate catalyst for methanol oxidation reaction. Nevertheless, Pt is not a good anode catalyst for methanol oxidation at normal temperature. Since it is enthusiastically poisoned by powerfully adsorbed intermediates, such that CO_{ads}. To promote the methanol electro-oxidation at platinum, modification of the catalyst surface has been made by the addition of a second metal to platinum [1-3].

The Pt–Ru/C binary metallic catalyst is commonly accepted as the best electrocatalyst for methanol oxidation due to its high CO tolerance, which can be achieved via its electronic effects and bifunctional mechanisms that improve the catalytic activities of electrochemical reactions. However, controversy exists concerning the real improvement of the methanol electro-oxidation reaction [4,5]. Despite the controversies, recent studies have shown that the Pt–Ru–Co/C catalyst has a

dramatic effect on its electrocatalytic activity. The enhanced activity of the ternary catalyst is due to the promoting effect of the second or third elements added to Pt. In the present study, we evaluated the catalytic activity for methanol oxidation reaction (MOR) by incorporating Co into Pt–Ru/MC catalysts in nonmembrane power system.

Experimental

Materials

The metal precursors used for the preparation of electrocatalysts were $\text{H}_2\text{PtCl}_6 \cdot 6\text{H}_2\text{O}$ (from Sigma Aldrich), $\text{RuCl}_3 \cdot 3\text{H}_2\text{O}$ (from Sigma Aldrich), and $\text{Co}(\text{NO}_3)_2 \cdot 6\text{H}_2\text{O}$ (from Sigma Aldrich). Mesoporous carbon (from Cabot Corp.,) was used as a support for the catalysts. Graphite plates (from E-TEK) were used as substrates for the catalyst to prepare the electrodes. Ethylene glycol (from Merck) was used as the solvent and reduction agent. Nafion[®] (DE 521, DuPont USA) dispersion was used to make the catalyst ink. Methanol (from Merck), sodium percarbonate (from Riedel) and H_2SO_4 (from Merck) were used as the fuel, the oxidant and as the electrolyte for electrochemical analysis, respectively. All the chemicals were of analytical grade. Pt/MC (40-wt%, from E-TEK) was used as the cathode catalyst.

Catalyst preparation

Carbon-supported catalysts containing Pt, Ru and Co with different atomic ratios were synthesized employing ethylene glycol (EG) as a reactant and reducing agent together with citric acid (CA) in line with the Pechini methodology. The Pt, Ru and Co precursors were prepared separately by employing metallic salts, namely, $\text{H}_2\text{PtCl}_6 \cdot 6\text{H}_2\text{O}$, $\text{RuCl}_3 \cdot 3\text{H}_2\text{O}$ and $\text{Co}(\text{NO}_3)_2 \cdot 6\text{H}_2\text{O}$, dissolved in a mixture of EG and CA at 70 °C and the mixture was kept under vigorous stirring for 2–3 h composing a polyester network that contains the metallic ions homogeneously distributed. The CA/EG/metal molar ratio is 4:16:1 for all the polymeric precursors. It appears that the citric chelate helps to prevent particle aggregation in a certain extent and induce nanoparticles to get high dispersion.

To obtain the supported catalysts, appropriate amounts of the polymeric precursors were dissolved in ethanol and a calculated amount of the functionalized mesoporous carbon

support was added. Finally, the mixture precursor solution/carbon was homogenized in an ultrasonic bath and then calcinated at different temperatures under an air atmosphere, using a temperature program reaching 400 °C to eliminate the excess carbon [6]. For comparison, the monometallic Pt/MC, and bimetallic Pt–Ru/MC and Pt–Co/MC catalysts were synthesized under the same conditions. The electrocatalytic mixtures and atomic ratios were $\text{Pt}_{60}\text{Ru}_{30}\text{Co}_{10}/\text{MC}$, $\text{Pt}_{60}\text{Ru}_{20}\text{Co}_{20}/\text{MC}$, $\text{Pt}_{60}\text{Ru}_{10}\text{Co}_{30}/\text{MC}$, $\text{Pt}_{50}\text{Ru}_{50}/\text{MC}$, $\text{Pt}_{50}\text{Co}_{50}/\text{MC}$ and $\text{Pt}_{100}/\text{MC}$. The nominal loading of metals in the electrocatalysts was 40 % wt and rest 60 % wt was mesoporous carbon.

Results and Discussion

Physical characterization

X-ray diffraction (XRD)

The XRD patterns of the prepared $\text{Pt}_{60}\text{Ru}_{30}\text{Co}_{10}/\text{MC}$, $\text{Pt}_{60}\text{Ru}_{20}\text{Co}_{20}/\text{MC}$, $\text{Pt}_{60}\text{Ru}_{10}\text{Co}_{30}/\text{MC}$, $\text{Pt}_{50}\text{Ru}_{50}/\text{MC}$, $\text{Pt}_{50}\text{Co}_{50}/\text{MC}$ and $\text{Pt}_{100}/\text{MC}$ catalysts are shown in Fig. 1.

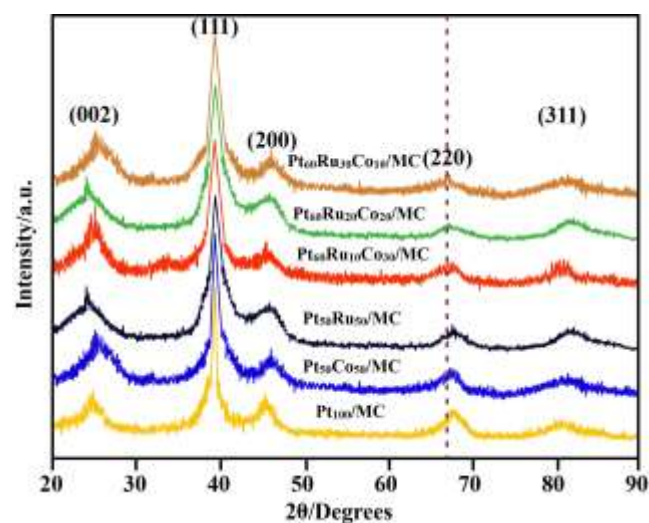


Fig. 1. X-ray diffraction patterns of $\text{Pt}_{60}\text{Ru}_{30}\text{Co}_{10}/\text{MC}$, $\text{Pt}_{60}\text{Ru}_{20}\text{Co}_{20}/\text{MC}$, $\text{Pt}_{60}\text{Ru}_{10}\text{Co}_{30}/\text{MC}$, $\text{Pt}_{50}\text{Ru}_{50}/\text{MC}$, $\text{Pt}_{50}\text{Co}_{50}/\text{MC}$ and $\text{Pt}_{100}/\text{MC}$ catalysts.

The first peak located at around 25° in all the XRD patterns is attributable to the Vulcan mesoporous carbon support. The 2θ of the (2 2 0) peak for $\text{Pt}_{60}\text{Ru}_{30}\text{Co}_{10}/\text{MC}$, $\text{Pt}_{60}\text{Ru}_{20}\text{Co}_{20}/\text{MC}$, $\text{Pt}_{60}\text{Ru}_{10}\text{Co}_{30}/\text{MC}$, $\text{Pt}_{50}\text{Ru}_{50}/\text{MC}$ and $\text{Pt}_{50}\text{Co}_{50}/\text{MC}$ shows a higher angle shift than the characteristics of face-centered cubic (fcc) crystalline Pt at 2θ values of 39°, 47°, 67° and 82° and are indexed with planes (1 1 1), (2 0 0), (2 2 0) and (3 1 1), respectively, indicating that the electrocatalysts have good alloy formations

and suggesting the effect of a different atomic rate of Co in the ternary catalyst. No diffraction peaks were attributed to pure ruthenium and cobalt or ruthenium rich hexagonal close packed (hcp) phase, appear in the XRD patterns, suggesting that ruthenium and cobalt atoms either form an alloy with platinum or exist as amorphous oxide phases. The Pt–Co/MC electrocatalyst also showed the same characteristic peak as that of the Pt–Ru/MC electrocatalysts. The fcc lattice parameters were evaluated from the angular position of the (2 2 0)

peaks, which reflect the formation of a solid solution (Table 1). The decrease in lattice parameters of the alloy catalysts reflects the progressive increase in the incorporation of Ru and Co into the alloyed state. The difference of lattice parameters and the shift of (2 2 0) plane indicate interactions between Pt, Ru and Co. The average particle size for Pt–Ru/MC, Pt–Co/MC, and Pt–Ru–Co/MC electrocatalysts were in the range of 3-4.5 nm was estimated using the Scherrer equation.

Table 1. The EDX composition, lattice parameters, and the particle size obtained for different atomic ratios of electrocatalysts

Electrocatalyst	Nominal Atomic ratio			EDX Atomic ratio			Lattice parameter (nm)	Crystallite size (nm)	Particle size from TEM (nm)
	Pt	Ru	Co	Pt	Ru	Co			
Pt/MC	100	-	-	99	-	-	0.3915	4.3	4.1
Pt–Co/MC	50	-	50	51	-	49	0.3902	4.2	3.9
Pt–Ru/MC	50	50	-	52	48	-	0.3888	3.7	3.4
Pt–Ru–Co/MC	60	10	30	62	9	29	0.3901	3.6	3.3
Pt–Ru–Co/MC	60	20	20	62	19	19	0.3898	3.4	3.2
Pt–Ru–Co/MC	60	30	10	62	29	9	0.3896	3.2	3.0

Transmission Electron Microscopy (TEM)

TEM image of the Pt–Ru–Co/MC alloy catalysts and the corresponding particle size distribution histogram are presented in Fig. 2. From the TEM images, the average particle diameter was found to be approximately 3-4 nm, which is in fairly good agreement with the data calculated from XRD. The particle size distribution of these catalysts is shown in Table 1 in accordance to the TEM images.

Energy Dispersive X-ray Spectroscopy (EDX)

Energy dispersive X-ray spectroscopy is conducted by focusing the electron beam on several different selected regions of the carbon supported Pt–Ru–Co nanoparticles. An EDX spectrum of Pt–Ru–Co/MC nanoparticle is shown in Fig. 3. The average composition of the sample was in atom ratio of Pt:Ru:Co = 6:3:1. The EDX results of the binary Pt–Ru/MC and Pt–Co/MC and the ternary Pt–Ru–Co/MC catalysts are very close to the nominal values, which indicate that the metals were loaded onto the mesoporous carbon support without obvious loss.

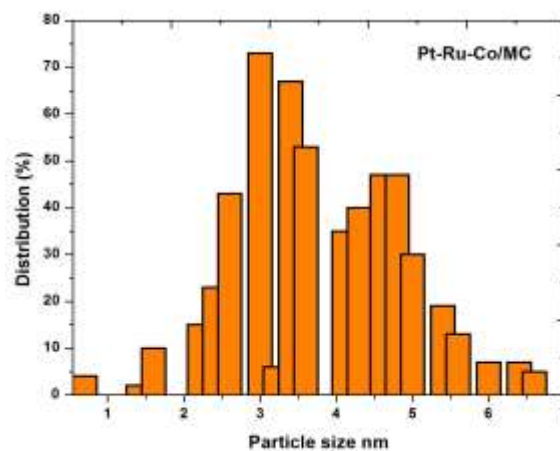
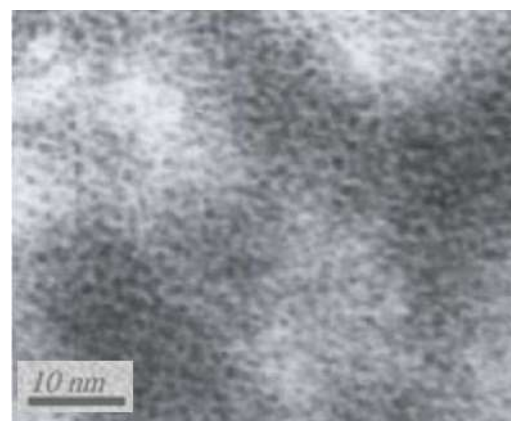


Fig. 2. TEM image and particle size distribution of Pt–Ru–Co/MC catalyst

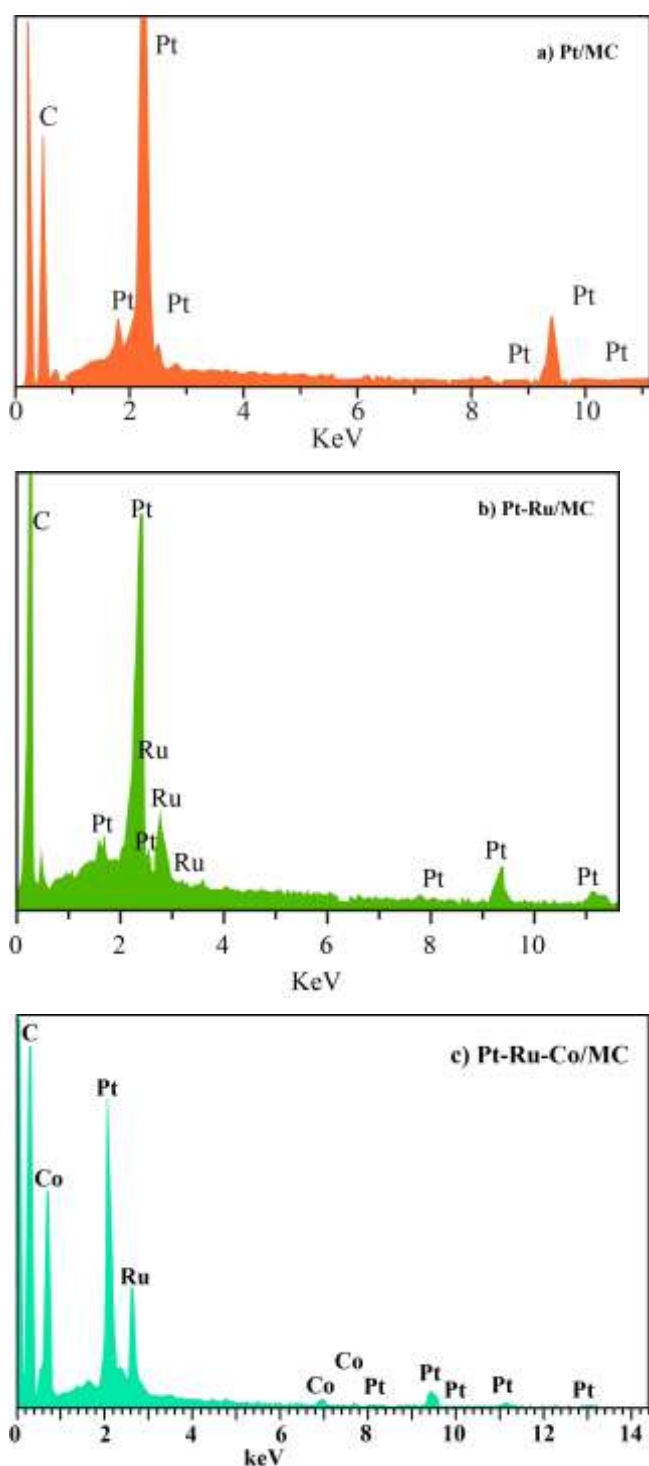


Fig. 3. EDX spectra of (a) Pt/MC, (b) Pt–Ru/MC and (c) Pt–Ru–Co/MC catalysts

Electrochemical Characterization

Cyclic Voltammetry

Fig. 4 shows the cyclic voltammogram (CV) on the Pt₆₀Ru₃₀Co₁₀/MC, Pt₆₀Ru₂₀Co₂₀/MC, Pt₆₀Ru₁₀Co₃₀/MC, Pt₅₀Ru₅₀/MC, Pt₅₀Co₅₀/MC and Pt₁₀₀/MC catalysts for CO oxidation in a solution of 0.5 M H₂SO₄. Due to the strong adsorption of CO onto

the Pt surface, the hydrogen adsorption-desorption of the Pt was completely blocked in the hydrogen region; indicating the presence of a saturated CO adlayer [7,8].

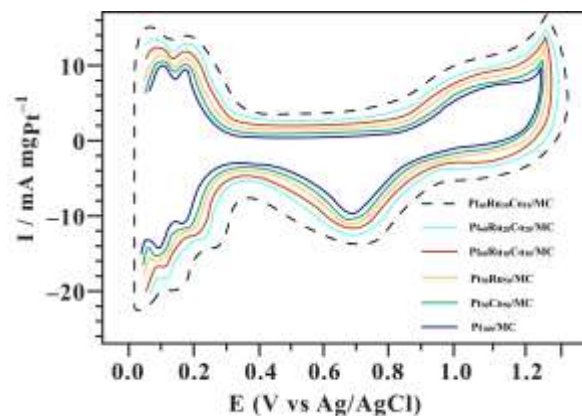


Fig. 4. CVs of Pt₆₀Ru₃₀Co₁₀/MC, Pt₆₀Ru₂₀Co₂₀/MC, Pt₆₀Ru₁₀Co₃₀/MC, Pt₅₀Ru₅₀/MC, Pt₅₀Co₅₀/MC and Pt₁₀₀/MC electrocatalysts in 0.5 M H₂SO₄.

The electrochemically active surface areas (SEAS) of the electrocatalysts were calculated using CO adsorption (SEAS/CO) and roughness of electrodes [9,10]. The roughness of each electrode is calculated by dividing SEAS obtained with the apparent surface area. Estimation of the electrode roughness and SEAS values are shown in Table 2. Based on these values, the highest electrochemically active area is achieved for the ternary electrocatalysts.

In comparison to pure Pt, the oxidation of CH₃OH_{ads} at Co containing Pt–Ru/MC surfaces exhibits a shift of the peak potential to lower potentials. The methanol oxidation evokes a quick formation of CO_{ads} at very low potentials, where CO_{ads} is not yet oxidized, and so hinders the further adsorption and decomposition of methanol. At potentials above the onset potential of the adsorbate oxidation, both parallel oxidation paths are taking place simultaneously. At a low potential, higher current efficiencies for CO₂ are observed on Pt–Ru–Co/MC electrodes than on pure Pt surfaces. This suggests that in presence of Co, Ru ad-atoms promote the reaction path via CO_{ads} in the low potential region. At higher potentials, the same current efficiency for CO₂ as on pure Pt indicates that the ternary Pt–Ru–Co/MC electrocatalysts loses its co-catalytic activity towards methanol oxidation. This loss of the activity is possibly caused by the formation of inactive anhydrous Ru oxide at higher potentials. The CV curves

were obtained in a half device between 0.05 and 1.2 V (vs. Ag/AgCl) in the absence of methanol. The characteristic features of polycrystalline Pt, i.e. hydrogen adsorption/desorption peaks in low potential region, oxide formation/stripping wave/peak in high potential region and a flat

double layer in between, are observed for all the synthesized catalysts. The voltammograms of the electrocatalysts did not display a well-defined hydrogen region between 0.05 and 0.35 V, as the catalyst's features in this region are influenced by their surface composition [11-14].

Table 2. Comparison of hydrogen desorption charge and carbon monoxide desorption charge, and its electrochemical active surface area (SEAS) and electrode roughness

Catalyst	$Q_{CO}/\mu C$	Electrode real	$S_{EAS/CO}$ Roughness	
		Surface area (cm^2)	$(m^2gPt^{-1})^a$	
Pt ₁₀₀ /MC	1260	2.9	29	83.0
Pt ₅₀ Co ₅₀ /MC	650	1.5	30	43.7
Pt ₅₀ Ru ₅₀ /MC	713	1.6	33	46.5
Pt ₆₀ Ru ₁₀ Co ₃₀ /MC	906	2.1	35	60.5
Pt ₆₀ Ru ₂₀ Co ₂₀ /MC	957	2.2	37	63.3
Pt ₆₀ Ru ₃₀ Co ₁₀ /MC	1007	2.3	39	66.1

Fig. 5 corresponds to representative CVs of methanol oxidation under acidic conditions (1.0 M CH₃OH and 0.5 M H₂SO₄) catalyzed by Pt₆₀Ru₃₀Co₁₀/MC, Pt₆₀Ru₂₀Co₂₀/MC, Pt₆₀Ru₁₀Co₃₀/MC, Pt₅₀Ru₅₀/MC, Pt₅₀Co₅₀/MC and Pt₁₀₀/MC catalysts. The onset potential for the oxidation of methanol in a positive scan was a key factor for evaluating the catalyst activity [15]. The onset potentials for the oxidation of methanol on the Pt₆₀Ru₃₀Co₁₀/MC (0.23 V), Pt₆₀Ru₂₀Co₂₀/MC (0.28 V) and Pt₆₀Ru₁₀Co₃₀/MC (0.30 V) electrocatalysts were slightly lower than that on the Pt₅₀Ru₅₀/MC (0.34 V), Pt₅₀Co₅₀/MC (0.35 V) and Pt₁₀₀/MC (0.41 V) catalysts. All the current values were normalized by the geometric surface area of the electrode used. The CV curves depict the presence of a peak in the potential range of the positive sweep and another peak in the negative sweep. The peak in the positive sweep is associated with the methanol oxidation, and the peak in the negative sweep is related to the oxidation of carbonaceous intermediate products from incomplete methanol oxidation.

The peak current densities of Pt₆₀Ru₃₀Co₁₀/MC, Pt₆₀Ru₂₀Co₂₀/MC, Pt₆₀Ru₁₀Co₃₀/MC, Pt₅₀Ru₅₀/MC, Pt₅₀Co₅₀/MC and Pt₁₀₀/MC catalysts are 44.0, 41.4, 38.6, 37.2, 35.3 and 11.2 mA/cm², respectively, showing that the activity of the ternary Pt₆₀Ru₃₀Co₁₀/MC catalyst is a factor of ~3 times higher than that of

the Pt/MC catalyst. Table 3 summarizes the CV results of Pt₆₀Ru₃₀Co₁₀/MC, Pt₆₀Ru₂₀Co₂₀/MC, Pt₆₀Ru₁₀Co₃₀/MC, Pt₅₀Ru₅₀/MC, Pt₅₀Co₅₀/MC and Pt₁₀₀/MC electrocatalysts including the positive peak potentials and the corresponding peak current densities of MOR. The CV results show that pure Pt₁₀₀/MC catalysts do not behave as an appropriate anode for MOR due to its poisoning by strongly adsorbed intermediates such as CO. However, the introduction of Ru and Co promotes the electrocatalytic activity.

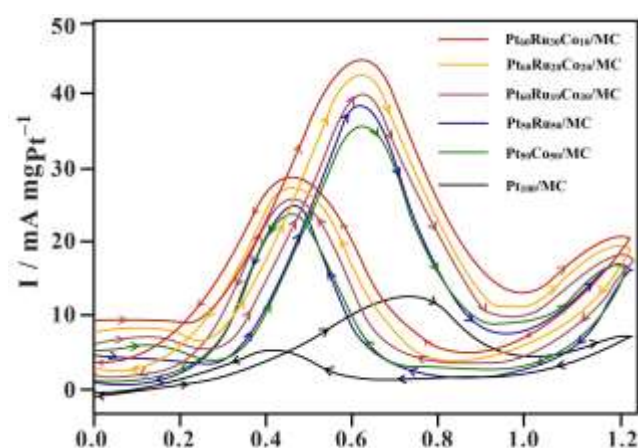


Fig. 5. CVs of Pt₆₀Ru₃₀Co₁₀/MC, Pt₆₀Ru₂₀Co₂₀/MC, Pt₆₀Ru₁₀Co₃₀/MC, Pt₅₀Ru₅₀/MC, Pt₅₀Co₅₀/MC and Pt₁₀₀/MC electrocatalysts in 1.0 M methanol + 0.5 M H₂SO₄

Table 3. CV results of Pt₆₀Ru₃₀Co₁₀/MC, Pt₆₀Ru₂₀Co₂₀/MC, Pt₆₀Ru₁₀Co₃₀/MC, Pt₅₀Ru₅₀/MC, Pt₅₀Co₅₀/MC and Pt₁₀₀/MC electrocatalysts

Catalyst	Positive peak potential (mV vs. Ag/AgCl)	Scan rate 50 mV s ⁻¹
		Peak current density (mA/cm ²)
Pt ₁₀₀ /MC	740	12.2
Pt ₅₀ Co ₅₀ /MC	622	36.3
Pt ₅₀ Ru ₅₀ /MC	616	38.2
Pt ₆₀ Ru ₁₀ Co ₃₀ /MC	613	39.6
Pt ₆₀ Ru ₂₀ Co ₂₀ /MC	612	42.4
Pt ₆₀ Ru ₃₀ Co ₁₀ /MC	609	45.0

Chronoamperometry

Fig. 6 shows the current densities measured at a constant potential jumping from 0.05 to 1.2 V in 1.0 M methanol+0.5 M H₂SO₄. The currents decay with time in a parabolic style and reach an apparent steady state within 80s. It can be seen that the current density of methanol electrooxidation on the Pt₆₀Ru₃₀Co₁₀/MC catalyst is higher than that on the Pt₆₀Ru₂₀Co₂₀/MC, Pt₆₀Ru₁₀Co₃₀/MC, Pt₅₀Ru₅₀/MC, Pt₅₀Co₅₀/MC and Pt₁₀₀/MC catalyst at the same potentials. The activity change for methanol oxidation decreases in the order of Pt₆₀Ru₃₀Co₁₀/MC > Pt₆₀Ru₂₀Co₂₀/MC > Pt₆₀Ru₁₀Co₃₀/MC > Pt₅₀Ru₅₀/MC > Pt₅₀Co₅₀/MC > Pt₁₀₀/MC, which is in fairly good agreement with our CV results. For the durability test, the chronoamperometric experiments were carried out at 0.05 to 1.2 V for 1000 s in the same conditions. Before each measurement, the solution was purged with high-purity nitrogen gas for at least 30 min to ensure oxygen-free measurements.

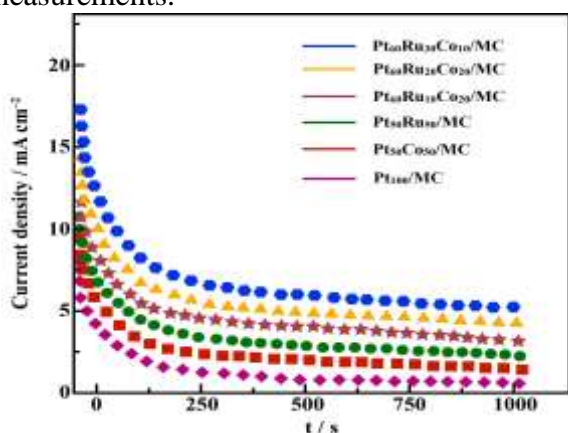


Fig. 6. CA of Pt₆₀Ru₃₀Co₁₀/MC, Pt₆₀Ru₂₀Co₂₀/MC, Pt₆₀Ru₁₀Co₃₀/MC, Pt₅₀Ru₅₀/MC, Pt₅₀Co₅₀/MC and Pt₁₀₀/MC electrocatalysts

Single device performance

The microfluidic architecture of laminar flow-based nonmembrane power systems overcomes the fuel crossover and water management issues that plague membrane-based power device and enables independent control of stream characteristics. Here we focused on maximizing device performance, in terms of power density, by tailoring various structural characteristics and catalytic activity of mesoporous carbon supported ternary Pt–Ru–Co catalysts. A single device performance was tested using Pt₆₀Ru₃₀Co₁₀/MC, Pt₆₀Ru₂₀Co₂₀/MC, Pt₆₀Ru₁₀Co₃₀/MC, Pt₅₀Ru₅₀/MC, Pt₅₀Co₅₀/MC and Pt₁₀₀/MC electrocatalysts as the anode. Polarization curves and power densities are shown in fig. 7. For each catalyst, the open-circuit voltages (OCV) were different, as would be expected in onset potentials. The OCVs of Pt₆₀Ru₃₀Co₁₀/MC, Pt₆₀Ru₂₀Co₂₀/MC, Pt₆₀Ru₁₀Co₃₀/MC, Pt₅₀Ru₅₀/MC, Pt₅₀Co₅₀/MC are higher than that of Pt₁₀₀/MC, 0.53 V, and the order of OCV is exactly same as the onset potentials.

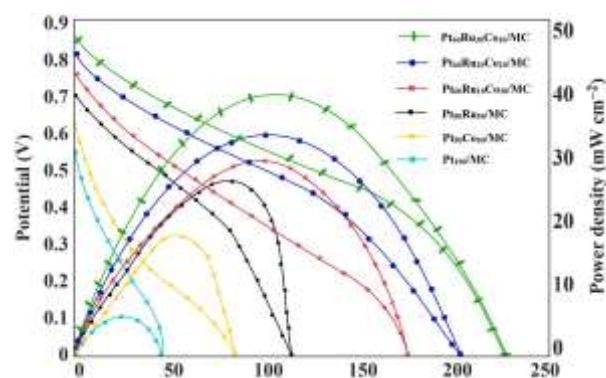


Fig. 7. Polarization and power density curves of Pt₆₀Ru₃₀Co₁₀/MC, Pt₆₀Ru₂₀Co₂₀/MC, Pt₆₀Ru₁₀Co₃₀/MC, Pt₅₀Ru₅₀/MC, Pt₅₀Co₅₀/MC and Pt₁₀₀/MC electrocatalysts

The OCV of Pt₆₀Ru₃₀Co₁₀/MC is the highest value of 0.87 V, which is approximately 0.33 V higher than that of Pt₁₀₀/MC. This indicates that Pt₁₀₀/MC is more rapidly poisoned by CO than any other alloy catalyst and that the oxidation of adsorbed CO is enhanced by the second or third metal. In the case of Pt₆₀Ru₃₀Co₁₀/MC the overall performance is superior to that of the bimetallic electrocatalysts. The maximum power densities obtained for Pt₆₀Ru₃₀Co₁₀/MC, Pt₆₀Ru₂₀Co₂₀/MC, Pt₆₀Ru₁₀Co₃₀/MC, Pt₅₀Ru₅₀/MC, Pt₅₀Co₅₀/MC and Pt₁₀₀/MC are 39.9, 33.6, 29.7, 28.2, 19.4 and 6.1 mW cm⁻², respectively (Table 4). We conclude that the substitution of a small amount of Co for Ru aids in cleaning surfaces poisoned by CO and provides additional reaction sites for methanol oxidation.

In nonmembrane power systems, pure Pt/MC catalyst does not behave as a very good anode for methanol electro-oxidation due to its poisoning by strongly adsorbed intermediates such as CO [16]. The binary and ternary electrocatalysts performed better than Pt/MC for methanol oxidation. Moreover, when the binary electrocatalysts were compared to the ternary ones in terms of oxidation the latter catalysts gave the best electrical performances. On the other hand, addition of Co to Pt (Pt–Co/MC) had a little effect, whereas addition of Co to Pt–Ru greatly enhanced the electrocatalytic activity.

As mentioned in our previous studies, the performance of the developed nonmembrane power system enhanced profoundly if the concentration of oxidant in cathodic stream is 10 times larger, and the current density is also increased approximately ten times [17-20].

Table 4. Summary of performance of single fuel device tests

Anode catalysts	Open circuit Voltage (V)	Maximum power density (mW cm ⁻²)	Maximum current density (mA cm ⁻²)
Pt ₁₀₀ /MC	0.53	6.0	48.1
Pt ₅₀ Co ₅₀ /MC	0.62	19.2	87.0
Pt ₅₀ Ru ₅₀ /MC	0.70	28.1	109.2
Pt ₆₀ Ru ₁₀ Co ₃₀ /MC	0.77	29.6	175.7
Pt ₆₀ Ru ₂₀ Co ₂₀ /MC	0.81	33.5	200.0
Pt ₆₀ Ru ₃₀ Co ₁₀ /MC	0.86	39.8	225.3

Conclusions

In this work, the study of methanol oxidation on mesoporous carbon-supported Pt–Ru–Co ternary nanoparticles has revealed details concerning the activity and stability of the catalysts in nonmembrane power systems. The maximum activity for methanol oxidation was found for the Pt₆₀Ru₃₀Co₁₀/MC than the Pt₆₀Ru₂₀Co₂₀/MC, Pt₆₀Ru₁₀Co₃₀/MC, Pt₅₀Ru₅₀/MC, Pt₅₀Co₅₀/MC and Pt₁₀₀/MC. The significantly enhanced catalytic activity for methanol oxidation can be attributed to the high dispersion of ternary catalysts and to Co acting as a promotion agent. XRD results show the homogenous alloy structure of Pt, Ru and Co. The TEM images indicated an average size of ternary nanoparticles of 3–4 nm. The atom ratio of Pt, Ru and Co from EDX analyses is close agreement with the original precursor concentration. The composition of ternary nanoparticles can be conveniently controlled by adjusting the initial metal salt solution and preparation conditions. The electrochemical

experiments showed that the Pt₆₀Ru₃₀Co₁₀/MC nanoparticles have higher catalytic activity than that of the other catalysts. We expect that the nonmembrane power system may be a promising candidate for practical power device to establish a clean and sustainable energy future. Further work is necessary to characterize the catalysts using different surface analysis techniques and to conduct tests of these electrocatalysts in microfluidic nonmembrane power systems.

Conflicts of interest

Authors declare no conflict of interest.

References

- [1] Ma J, Sahai Y, Rudolph RG. Direct borohydride fuel cell using Ni-based composite anodes. *J Power Sources* 2010; 195(15):4709-4713.
- [2] De Leon CP, Walsh FC, Pletcher D, Browning DJ, Lakeman JB. Direct borohydride fuel cells. *J Power Sources* 2006;155(2):172-181.

- [3] Wee JH. Which type of fuel cell is more competitive for portable application: direct methanol fuel cells or direct borohydride fuel cells?. *J Power Sources* 2006;161(1):1-10.
- [4] Shukla AK, Jackson CL, Scott K, Raman RK. An improved-performance liquid-feed solid-polymer-electrolyte direct methanol fuel cell operating at near ambient conditions. *Electrochim Acta* 2002;47(21):3401-3407.
- [5] Mitrovski SM, Elliott LCC, Nuzzo RG. Microfluidics devices for energy conversion; planar integration and performance of a passive, fully-increased H₂-O₂ fuel cell. *Langmuir* 2004;20(17):6974-6976.
- [6] Mitrovski SM, Nuzzo RG. A passive microfluidic hydrogen-air fuel cell with exceptional stability and high performance. *Lab on a Chip* 2006;6(3):353-361.
- [7] Choban ER, Waszczuk P, Kenis PJA. Characterization of limiting factors in laminar flow-based membraneless microfuel cell. *Electrochem Solid State Lett.* 2005;8(7):A348-A352.
- [8] Cheng H, Scott K. Influence of operating conditions on direct borohydride fuel cell performance. *J Power Sources.* 2006;160(1):407-412.
- [9] Duteanu N, Vlachogiannopoulos G, Shivhare MR, Yu EH, Scott K. A parametric study of a platinum ruthenium anode in a direct borohydride fuel cell. *J Appl Electrochem.* 2007;37(9):1085-1091.
- [10] Li ZP, Liu BH, Arai K, Asaba K, Suda S. Evaluation of alkaline borohydride solutions as the fuel for fuel cell. *J Power Sources* 2004;126(2):28-33.
- [11] Sung W, Choi JW. A membraneless microfuel cell using non-noble catalysts in alkaline solution. *J Power Sources* 2007;172(1):198-208.
- [12] Vijayaramalingam K, Kiruthika S and Muthukumaran B. Promoting Effect of Third Metal (M = Ni, Mo and Rh) on Pd–Ir Binary Alloy Catalysts in Membraneless Sodium Perborate Fuel Cells. *International Journal of Modern Science and Technology* 2016;1(7):257-263.
- [13] Kalaikathir SPR, Begila David S. Synthesis and characterization of nanostructured carbon-supported Pt electrocatalysts for membraneless methanol fuel cells. *International Journal of Modern Science and Technology* 2016;1(6):199-212.
- [14] Kjeang E, Djilali N, Sinton D. Microfluidic fuel cells; A review. *J Power Sources* 2009;186(2):353-369.
- [15] De Jong J, Lammertink RGH, Wessling M, Membraneless and microfluidic: a review. *Lab on a chip.* 2006;6:1125-1139.
- [16] Santos DMF, Sequeira CAC. Sodium borohydride as a fuel for the future. *Renew Sustain Energ Rev.* 2011;15(8):3980-4016.
- [17] Santos DMF, Sequeira CAC. On the electrosynthesis of sodium borohydride. *Int J Hydrogen Energy.* 2010;35(18):9851-9861.
- [18] Priya M, Elumalai M, Kiruthika S and Muthukumaran B. Influences of supporting materials for Pt-Ru binary catalyst in Ethanol fuel cell. *International Journal of Modern Science and Technology* 2016;1(1):5-11.
- [19] Mahendran S, Anbuselvan C. Kinetics and mechanism of oxidation of 5-(4'-bromophenyl)-5-oxopentanoic acid by acid permanganate, *International Journal of Modern Science and Technology* 2016;3(1):106-110.
- [20] Elumalai M, Priya M, Kiruthika S, Muthukumaran B, Effect of acid and alkaline media on membraneless fuel cell using sodium borohydride as a fuel. *J Afinidad* 2015;72:572.
